Delft University of Technology

Acoustic Side-Channel Communications for Aerial Drones with HUM

Sharma, Suryansh; Lica, Robert; Prasad, Venkatesha; Mottola, Luca; Ambroziak, Leszek

Citation (APA)
Sharma, S., Lica, R., Prasad, V., Mottola, L., & Ambroziak, L. (2024). Acoustic Side-Channel Communications for Aerial Drones with HUM. In *SenSys 2024 - Proceedings of the 2024 ACM Conference on Embedded Networked Sensor Systems* (pp. 267-280). (SenSys 2024 - Proceedings of the 2024 ACM Conference on Embedded Networked Sensor Systems). ACM. https://doi.org/10.1145/3666025.3699337

Important note
To cite this publication, please use the final published version (if applicable).
Please check the document version above.

Acoustic Side-channel Communications
for Aerial Drones with HUM

Suryansh Sharma
Networked Systems, TU Delft
Delft, Netherlands
suryansh.sharma@tudelft.nl

Robert Lica
Networked Systems, TU Delft
Delft, Netherlands
r.m.lica-1@student.tudelft.nl

R. Venkatesha Prasad
Networked Systems, TU Delft
Delft, Netherlands
r.r.venkateshaprasad@tudelft.nl

Luca Mottola
Politecnico di Milano, RI.SE, and
Uppsala University
Italy and Sweden
luca.mottola@polimi.it

Leszek Ambroziak
Bialystok University of Technology
Bialystok, Poland
l.ambroziak@pb.edu.pl

ABSTRACT

We present **HUM**–**H**igh-frequency **U**AV **M**essaging: an acoustic side channel communication system we design for localized drone-to-drone communications. We generate Pulse Width Modulated (PWM) signals from drone motors to carry information and improve communication reliability by mitigating propeller noise interference through modifications to the propeller's physical design. These modifications reduce propeller noise in the designated acoustic spectrum by up to 7 dB. We deploy a custom ultrasonic microphone shield specifically designed for decoding in the receiver. HUM's improved signal-to-noise ratio enables up to 80x higher data rates compared to the existing design from the literature while providing better scalability. HUM supports simultaneous decoding across 16 drones within 8 m, range as seen in real flight tests. The cost of this performance is minimal; we experimentally demonstrate that HUM has a marginal impact on flight dynamics and battery life.

CCS CONCEPTS

• **Computer systems organization** → *Embedded systems*; *Sensors and actuators*; **Robotics**; • **Hardware** → **Sound-based input / output**.

KEYWORDS

UAV, drones, robot-robot communication, swarming, side channels, audio processing, acoustic communication.

Figure 1: HUM communication: we use motors as transmitters, custom changes to existing propellers to reduce interference noise, an ultrasonic microphone at the receiver, and a dedicated communication protocol. A demonstration video can be found online: https://youtu.be/Ji_CjWFnaB4

1 INTRODUCTION

Aerial drones are now recognized as formidable mobile computing platforms [38]. They enable a multitude of applications [4, 21], including aerial mapping and surveillance [42], search and rescue [56, 59], environment monitoring [27, 45], and gas leak detection [13]. In indoor settings, micro- and nano-drones are deployed to support warehouse management tasks [18, 66], ambient intelligence applications [5], and human-drone interactions [19]. Owing to their size and energy consumption, micro- and nano-drones are extremely resource-constrained.

In many applications involving multiple drones, localized and short-range communication supports drone coordination in a shared physical space [43]. Most often, these systems use RF technologies such as Bluetooth and 802.15.4 [37, 57].

Where RF fails. Paradigmatic scenarios exist, however, where RF technologies fall short of expectations. During *Fukushima nuclear disaster*, the robots deployed in response encountered significant RF communication problems caused by high radiation levels and

the complex environment within the nuclear power plant. These interfered with the wireless control signals used by the robots [24] and forced rescue teams to rely on tethered connections, making operations much more challenging. Several reports indicate that, in addition to physical and environmental obstacles, reliable RF communication was a major hurdle in the effective deployment of robots in such hazardous areas [7, 11].

Jamming attacks on RF communications that impede the safe operation of drones are also increasingly reported [16, 29, 68, 75]. Intentional jamming of RF links is very common, for example, in military applications where adversaries may use special equipment to block RF communications [6, 17, 49, 53]. After natural disasters, RF communication could be blocked by infrastructure failures or terrain [47, 50, 62]. Temporary RF blackouts may also occur in challenging environments like warehouses, underground caves, or near high-voltage transmission lines, where RF signals can be dampened, absorbed, or scattered [23].

These scenarios require the use of *non-RF side channels* for *localized communications* that can, even with reduced capacity, be useful for coordination and contention while being interference agnostic. While each drone runs its own flight control loop locally, short-range non-RF communication can help drones in close proximity exchange critical navigation data or maintain formation. A key example is the implementation of an identification system "Friend or Foe" (iFF) to enable drones to distinguish between friendly and unauthorized drones [40]. This functionality is fundamental to preventing collisions and improving coordination in densely populated airspaces [40] and is increasingly required by drone regulations worldwide [3, 20] preferably using a different channel.

Challenges. Provisioning a non-RF communication channel for localized drone-to-drone communications is arguably difficult. Attempts exist in the literature that still provide insufficient bandwidth in many of the above scenarios and are inherently limited to sending a few heartbeat messages [10].

The key requirements we elicit are: ❶ scaling to more than a handful of drones to support applications from warehouse management to monitoring of high-voltage transmission lines; ❷ effectively supporting robot coordination and possibly operating as a fail-over link using non-RF technologies and with higher data rates than a couple of bits per second [10] to be able to send important parameters for coordination in one frame; ❸ reaching at least a few meters to reach drones operating in a shared physical space; ❹ only relying on the constrained resources found in micro- and nano-drones, thus limiting processing overhead, energy consumption, and additional weight that may impact the drone flight dynamics.

Attempts already exist to tackle *some* of these requirements, as we discuss in Sec. 2. For example, Bleep [10] utilizes propellers generating acoustic chirps with data rates up to 1-2 bps and a maximum of 4 coordinating drones, because the issue of propeller-generated noise greatly complicates decoding. However, Bleep [10] evidently struggles fulfilling the requirements ❶ and ❷.

Solution. We present a unique design called **HUM**–**H**igh-frequency **U**AV **M**essaging, which uses acoustic communications to meet these requirements. Fig. 1 shows a high-level overview. We generate Pulse Width Modulated (PWM) signals by purposely switching the frequency of drones' motors simultaneously, reducing the amplitude

of self-noise for reliable communication. We deploy a dedicated hardware shield with an ultrasonic microphone at the receiver that adds minimal weight. Three key technical contributions concur to make our design ultimately efficient:

(1) **A quantitative analysis** of the acoustic signals generated by micro- and nano-drones, including the propellers' noise and its effect on an acoustic signal possibly generated by modulating the PWM motor signals, illustrated in Sec. 3;

(2) **A custom design** of micro- and nano-drone propellers reducing the noise they generate upon intentionally generated drone motor audio signals, discussed in Sec. 4;

(3) **A dedicated communication protocol,** enabling scalable drone-to-drone communications by simultaneously modulating PWM signals of all four motors, generating orthogonal frequencies to increase the bit rate, described in Sec. 5.

The experimental evaluation in Sec. 6 indicates that HUM enables up to 80x higher data rates than existing designs, using all four motors as transmitters simultaneously utilizing four different frequencies while providing better overall scalability. For example, it can support simultaneous decoding of frames from 16 nearby drones and communicate within an 8 m range, as seen in real flight tests. This enables applications that are otherwise unfeasible, such as those hinted earlier, that require rich information exchanges beyond simple "heartbeats" [10]. Nonetheless, the cost for this performance is minimal: we demonstrate that HUM imposes a maximum of 7% overhead on battery life when a drone transmits data using the side channel for coordination exclusively. Note that side-channel communication is not needed continuously.

2 RELATED WORK

Our work touches upon several interrelated areas. We briefly survey relevant works next.

Acoustic communication. Recent literature explores the use of audio signals to carry information, employing off-the-shelf microphones in smartphones or wearables [39, 70–73].

Several works specifically investigate the use of acoustic side-channels to extract information leaked by electro-mechanical devices such as keyboards [8, 33] and printers [9]. Smart devices like Secure-Vibe [30] and Deaf-Aid [22] employ audio signals generated by vibrating motors as a dedicated communication channel. Their design primarily focuses on leveraging acoustic signals covertly for communication or as a side channel to extract additional information. MotorBeat [64] uses household DC motors, like those in electric toothbrushes, to transmit acoustic messages to a smart speaker, achieved by randomizing the switching period of the PWM signal driving the motors. These motors, characterized by relatively low rotation speeds, differ significantly from drone motors due to higher rotational regimes and the presence of propellers.

Propeller noise. The noise emitted by drone motors during flight may serve functionality such as drone identification [48] or indoor localization and tracking [55, 65]. These systems do not aim to reduce propeller noise but instead leverage specific audio signatures generated by drones during hovering for decoding identity or location information. The transmitters are speakers carried by large drones. These designs are intended for scenarios where groups of
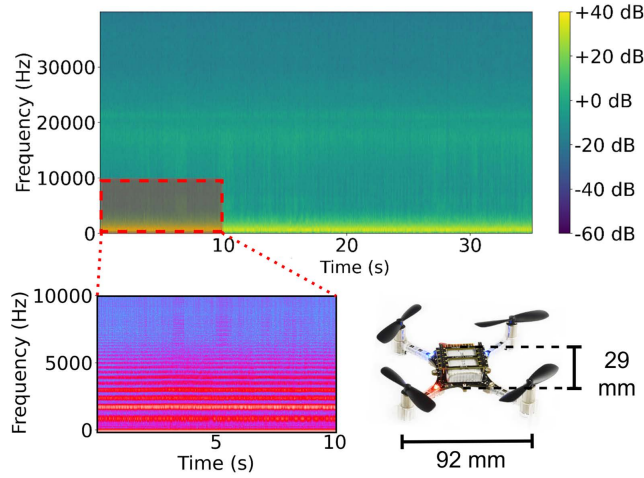
Figure 2: Spectrogram of noise generated by a CrazyFlie nano-drone as recorded by a MEMS microphone placed onboard.
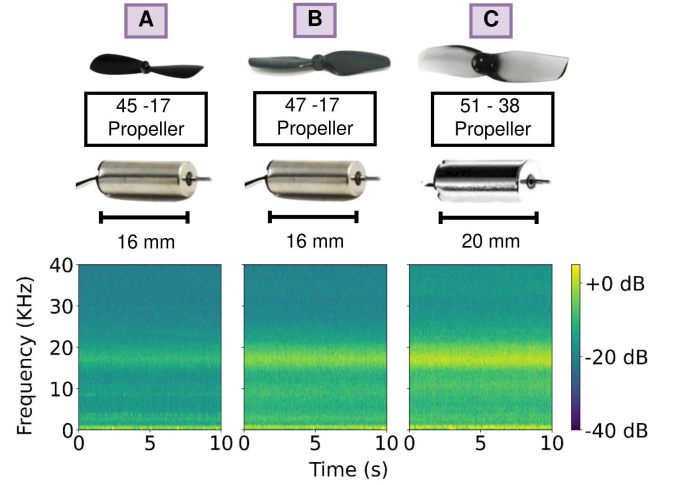

Figure 3: Noise generated by three different nano-drones with different motor-propeller geometries at 1 m distance. Each combination generates a different amount of noise in the 0-23 kHz spectrum.

heterogeneous drones fly together, each with a distinct audio signature. This work targets systems with multiple yet homogeneous collaborating micro- or nano-drones.

Manipulating the PWM frequency of drone motors is recognized as a way to generate audio signals [1]. Bleep [10] relies on this functionality to generate acoustic up- and down-chirps, achieving a 1-2 bps bit rate for heartbeat messaging and drone identification. Further opportunities exist within this framework, which we explore in this work, related to the characterization of the audio tone generation, the mitigation of noise coming from propellers, and the use of the ultrasonic part of the acoustic spectrum.

In the next section, we begin by quantitatively studying how to best exploit the phenomena of motor-generated audio signaling and, at the same time, how to mitigate propeller-generated noise to improve communication. In doing so, we build the necessary technical foundation for the rest of the paper.

3 AEROACOUSTICS

We target micro- and nano-drones of 10-25 cm in diameter and weighing from 50 g to 500 g, which are the most common ones for indoor applications. These typically employ brushed coreless motors rated at a few watts of power [52].

3.1 Understanding Drone Noise

Propellers create pressure waves, and the motor casing vibrates, generating noise when drones operate. Propellers vary in shape and size, yet the underlying principles of generating noise are always the same. Propellers generate harmonic or tonal and broadband noise spread over a wide range of frequencies in the audio spectrum band and are typically induced by turbulence. This noise source is random and, therefore, unsteady.

We examine the physics leading to noise generation from a rotating propeller. As it spins, the pressure difference created between the propeller's top and bottom surfaces produces the *tonal* noise. *Broadband* noise, on the other hand, originates from the pressure

fluctuations on the propeller surface, particularly towards the leading edge [34]. On top of that, a Boundary Layer at the propeller surface may be the source of narrowband tones, called long boundary layer (LBL) noise, which may be observed as narrowband peaks when the propeller rotates.

Broadband noise is usually smaller compared to tonal noise components. Harmonic or tonal noise is periodic and can be split into *thickness* and *steady-loading* noise. Thickness noise is generated due to the displacement of air molecules by the volume of the propellers and increases with increasing rotational speed. Steady-loading noise, instead, stems from the pressure difference above and below the blades, which generates lift and drag. This type of noise is significant at low and moderate rotational regimes [25, 41].

By mapping the spectral frequencies of the propeller noise, we can determine the dominant frequencies and harmonics. Fig. 2 shows the broadband and tonal noise generated by the propeller of the popular CrazyFlie. We capture the audio signal using a MEMS microphone placed directly on the frame. The plot shows the entire spectrum, including frequencies up to 40 kHz. The noise is spread up to 25 kHz with strong tonal noise visible up to 6 kHz.

It becomes apparent that the specific motors and propellers affect the noise spectral signature. Fig. 3 shows the audio signal generated by different combinations of brushed DC motors and propellers. Note that the same combination results in an identical audio signature across different drones, changing only with changing motor and/or propellers. All combinations are usable with the CrazyFlie nano-drone. The noise produced by each combination differs in intensity, increasing with the increasing size of motors and propellers and their rotational speeds. In all of them, we observe prominent noise in the audible spectrum.
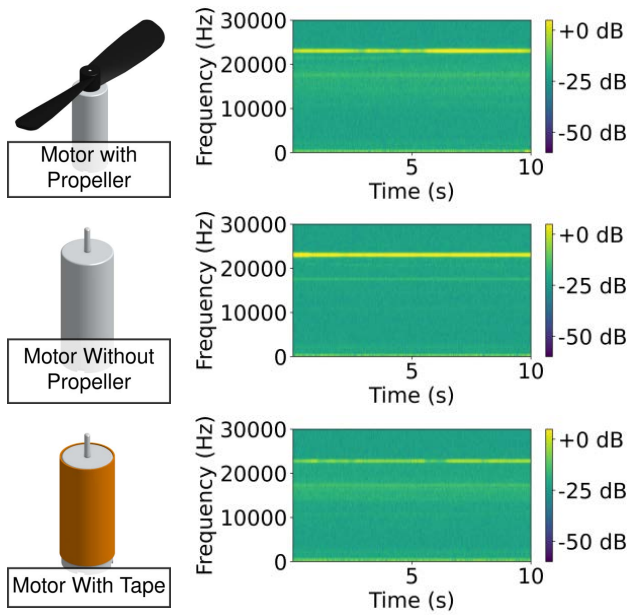
Figure 4: Spectrogram of motor generated hum of 23 kHz by modulating the PWM switching frequency on a 7x16 mm DC coreless drone motor with: (top) a mounted propeller; (middle) no propeller; and (bottom) additional tape to dampen the motor vibrations.

3.2 Motors as Audio Sources

Motor vibrations also contribute to the generated noise, even though the larger propeller noise often overshadows this. The continuously changing PWM signal makes the drone motor produce sounds at specific frequencies. The PWM signal has two properties influencing the generated sound: the duty cycle and frequency of the square wave. By changing the duty cycle, we change the duration of the ON time we send to the motor as a control signal. This changes their noise; however, the duty cycle is typically governed by the flight control logic responsible for flying the drone [14]. We can, instead, vary the square wave frequency, that is, the number of ON-OFF pulses itself, which is not determined by the flight control logic but instead set at a fixed value to produce different acoustic frequencies. We use this parameter to transmit different bits or symbols.

Changing the frequency of the motor PWM signal results in a hum as the motor casing and coils vibrate at a particular frequency. Fig. 4 shows the humming noise both with and without a propeller. The middle and bottom pictures demonstrate that the motor is causing the hum, generating the sound even when no propeller is attached and that the motor hum primarily depends on motor construction. Motor casing, housing, and coils resonate at different frequencies, generating a distinctive audio signal when powered. Fig. 4 also demonstrates that the intensity of the motor hum reduces when the vibration of the motor body is dampened, for example, using a thick layer of tape. The drone frame may also have a small dampening effect on the generated sound and may alter it if the motors are not properly secured.
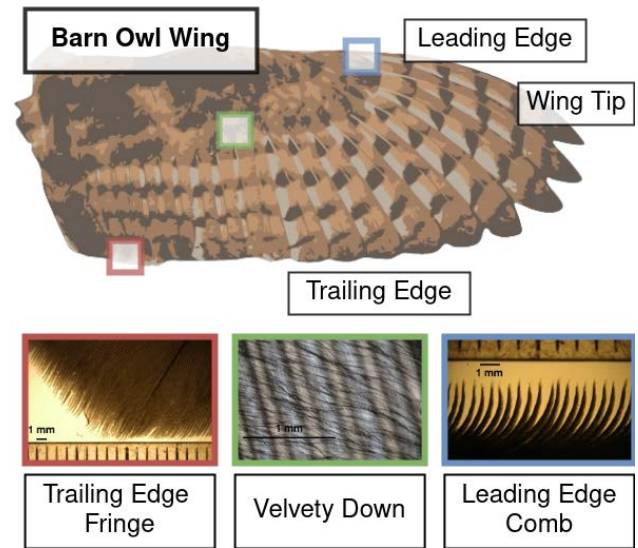

Figure 5: The noise suppressing wing morphology of a barn owl. Distinctive features at the wing edges and upper-wing surface contribute to the silent flight [28].

3.3 Self Interference

We employ the hum produced by altering the motor PWM signal frequency as the main means of communication. The propellers' audio signals become the main noise source, possibly inhibiting reliable communication. When a drone's motors generate the hum encoded with information, acting as transmitters, the propellers of each flying drone in the vicinity contribute to channel noise. Microphones that listen to this hum inevitably need to decode it in the presence of the background propeller noise. This is especially true when the microphone is placed right onboard the drone.

At the receiver end, the main source of interference is listening to the drone's propellers. This noise likely dominates the channel compared to the hum a distant transmitting drone produces. The key issue is reducing the "self-inflicted" noise of the drone. The next section illustrates how we do so.

4 TAMING PROPELLER NOISE

There are many works in the literature to reduce propeller noise [35, 36, 46, 54]. They focus on broadband noise and do not target denoising a specific part of the frequency spectrum. Since we can control the motor's transmitting audio frequency, we tune the system to utilize the part of the spectrum with reduced interference or stronger hum signals. Existing techniques reduce noise in the lower frequency bands whenever possible, pushing noise to higher frequencies that humans are less sensitive to. On the contrary, we are specifically interested in pushing propeller noise to the lower part of the frequency spectrum, freeing the higher frequency bands. We aim to do so with minimal additional hardware or major propeller re-designs [60].

Our inspiration is from nature: Barn owls are known to fly silently [69]. They can do so inches away from prey without being detected. This is possible because they have specialized plumage
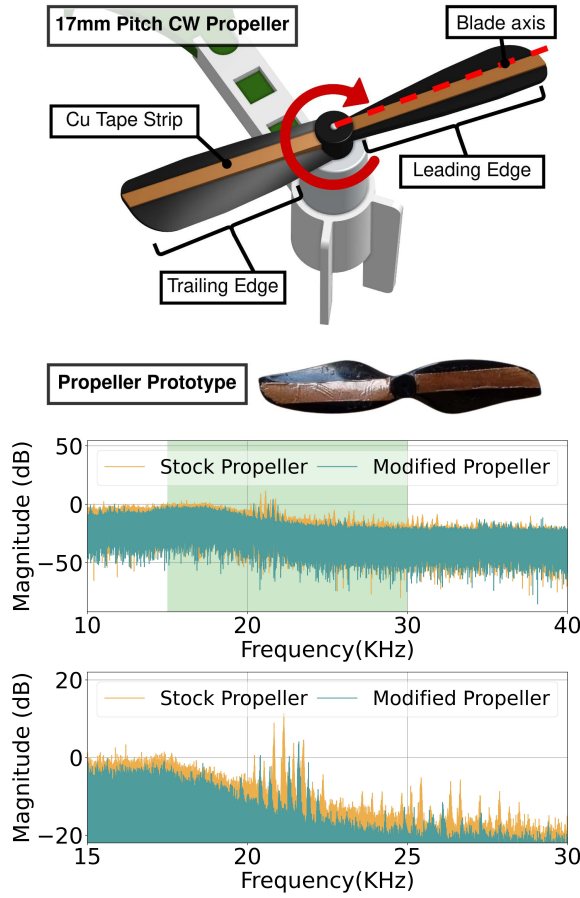
Figure 6: Propeller modification CAD diagram and the prototype (top); noise spectrum magnitude for the two propellers (middle, bottom) showing up to 7 dB reduction in self-noise.
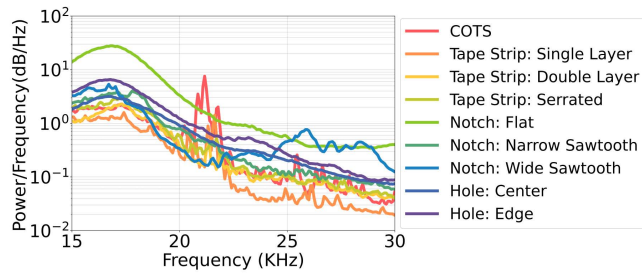

Figure 7: Different noise suppressing propeller modifications and their effect on the acoustic spectrum.

and wing features that eliminate the aerodynamic noise generated by the wings. Three key physical features contribute to the silent flight, shown in Fig. 5: *(1)* a comb of stiff feathers along the leading edge, *(2)* a flexible fringe at the trailing edge, and *(3)* a soft carpet-like material distributed on the wing top [28].

These natural adaptations influence the acoustic spectrum by altering the wind flow over their surface. They hint at what we can manipulate when modifying our propellers to subdue noise. Using leading or trailing edge modifications may be an effective strategy for reducing turbulent noise and, hence, some of the higher frequency components. We cannot, however, replicate the barn owl's wing features directly on small-sized and fast-moving propellers.

However, we combine these observations with the discussion on LBL noise of Sec. 3. The key insight we gain is that adding a small *boundary layer trip* can produce a large reduction in broadband noise in lightly loaded conditions [32].To this end, we use a leading edge boundary layer trip to force the boundary layer transition. Such uneven perturbations are also visible on the barn owl's wings and are believed to contribute to noise reduction [69].

We thus devised a deceptively simple modification to the drone propellers, which greatly reduces propeller noise in the 15 kHz to 25 kHz part of the audio spectrum. We add a 0.05 mm thick and 2 mm wide rectangular copper strip on each propeller blade along the length of the propeller, as shown in Fig. 6. The strip abates LBL self-noise by breaking down the aeroacoustic feedback loop generated when the LBL stretches for the entire length of the propeller chord and the propellers spin between 18,000 to 23,000 RPM. As a result, the spectrum magnitude of the modified propellers reduces up to 7 dB, as shown in Fig. 6. The additional weight is minimal, with no discernable effect on the static thrust generated and a negligible effect on lifetime, as we report in Sec. 6.

Copper strips can serve as a viable solution to enhance the mechanical properties of propeller blades, particularly in reducing vibrations and improving stiffness, damping, and mass distribution. Using copper improves the stiffness of the blades – which in turn alters the natural frequency – potentially reducing resonance effects that contribute to noise and mechanical stress. Copper's inherent damping properties help absorb and dissipate vibrational energy, making the propeller less susceptible to harmful vibrations. Additionally, increasing the mass distribution along the propeller blade by attaching copper strips may help shift the operating frequency away from any resonance conditions, reducing the likelihood of excessive vibrations. This approach is successfully applied in marine propellers to minimize vibrations and improve propulsion efficiency, showing similar potential for aerial propellers [15, 74]

We arrive at this design after considering several different options. These include making holes or notches of different shapes on the original CrazyFlie propellers or adding more than a single layer of copper tape. Each modification is based on insights gained from existing literature [32, 61, 67]. Fig. 7 experimentally demonstrates that our choice is best at freeing the higher frequency bands, which is precisely our goal. Some modifications, such as the flat notch, perform worse throughout the spectrum. Other solutions perform similarly to our design in the lower frequency bands but worse in the higher ones, where we seek the best performance. Our work in this area is one of the first to explore the effect of physical propeller modifications in the 40 kHz spectrum [35, 36, 46, 54].

5 DESIGNING HUM

The dedicated propeller design illustrated earlier is the stepping stone for HUM, whose design we explain here. The rest of the section specifically illustrates how we fulfil the four key requirements outlined in the Introduction section.
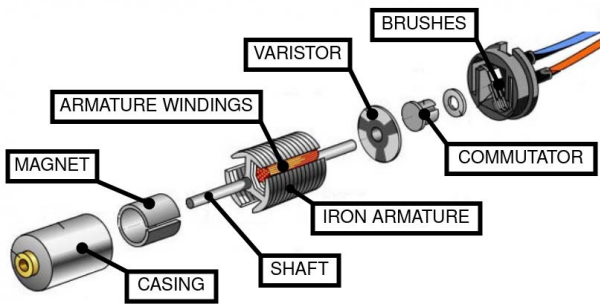
Figure 8: Exploded view of a typical DC drone motor. The changing current through the windings induces mechanical vibrations passing through the metal casing, producing an acoustic hum.

To make our discussion concrete, we consider the CrazyFlie 2.1 [12] nano-drone as the target platform on which we implemented and tested our design. The CrazyFlie is equipped with four 16 mm core-less DC motors with a KV value of 14000 RPM/V. A brushless motor's KV factor describes the relationship between the peak voltage and its rotation speed in a no-load condition. We use bi-blade 47 mm diameter polycarbonate propellers with a pitch of 17 mm. The entire drone is 92 mm wide diagonally and 29 mm in height. Its total dry weight is 27 g. It uses an nRF51822 radio and microcontroller to transmit telemetry information through a wireless 2.4 GHz link. A BMI088 6-axis IMU measures linear accelerations and angular velocities. The flight controller runs on an STM32F405 Cortex-M4 core with 192 kB SRAM. We customize the stock firmware with the release tag 2023.07.

Albeit the following discussion is centred on the CrazyFlie nano-drone, our design enjoys sufficient generality to apply to other drone platforms sharing similar features, such as the many nano-drones based on ESP32 chips [2].

5.1 Transmitter Design: Motor Actuation

We modulate the switching frequency of the PWM signal, driving the DC motors to transmit information. Fig. 4 demonstrates that the acoustic signals are due to the motor hardware, whereas the propeller does not contribute to the latter, as discussed in Sec. 3. This insight prompts us to examine the motor structure further.

Fig. 8 shows an exploded view of the components in a typical DC drone motor. Both cored, and coreless motors are equipped with brushes and a commutator. In the coreless case, the rotor windings are wrapped to form a self-supporting hollow cylinder that is typically epoxied. The humming sound is due to the current flowing through the windings, causing interactions with the permanent magnet. This induces resonance, leading to mechanical vibrations because of PWM switching.

The vibrations pass through the metal casing and yield acoustic tones. The flight controller is responsible for setting the desired thrust. In doing so, the only controllable parameter is the duration of the motor being ON. Most control systems use the PWM signal to modulate the power being delivered to the motor. This is achieved
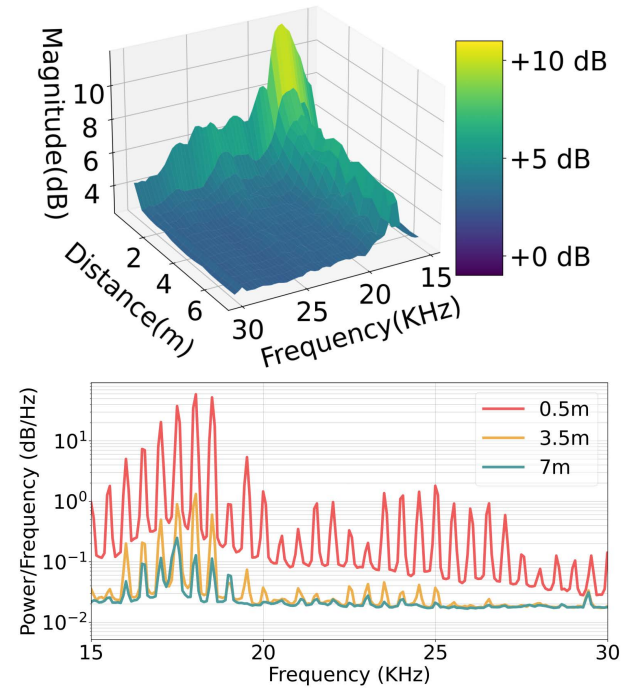

Figure 9: Magnitude of the spectrum (top) of drone motor produced hum with increasing distance. The drone produces hums in 500 Hz intervals from 10 kHz to 40 kHz. The power spectral density (bottom) of each frequency at three distances shows the effect of distance on each humming frequency.

by setting different values of pulse width, which regulate the time the motor is powered ON. The motor is not powered otherwise.

The PWM signal is normally a square wave with a fixed switching frequency. The flight controller makes fine adjustments to the power given to a motor to vary the thrust and consequently set the drone's three-dimensional attitude. This PWM-driven control is effective for inductive loads such as DC motors because the current in motor windings cannot be switched ON or OFF instantaneously. By solely changing the PWM frequency, we ensure not to alter the power setting determined by the flight controller and time but simultaneously set the acoustic frequency used to transmit the bits. We experimentally verify this argument in Sec. 6.

Note that different motors transmit different acoustic frequencies. As Fig. 4 shows, different mechanical properties make the motors resonate differently. This has an impact on the frequency of acoustic signals they can generate. Fig. 9 also shows the variation in the intensity of the motor-generated hum with distance. The plot indicates that the region between 15 kHz and 30 kHz features the highest intensity, corresponding to a higher signal-to-noise ratio. It also shows that at 3.5 m (7 m) distance, only the frequencies between 15 kHz and 25 kHz can be detected. Thus, we make different drones select different humming frequencies (signatures) using different PWM frequencies, which allows them to co-exist.
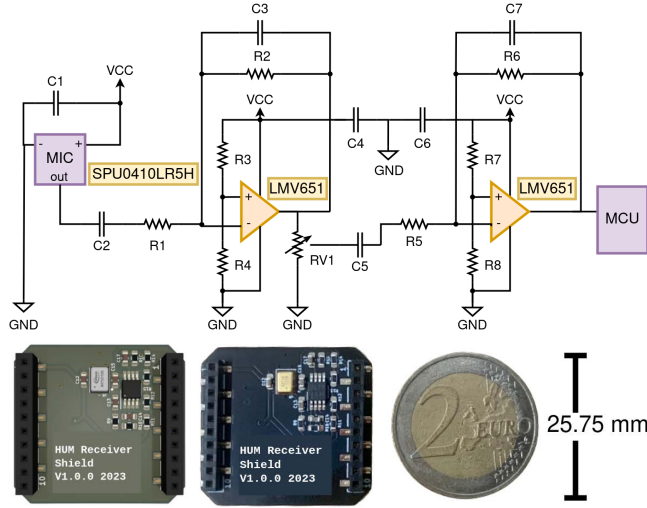
Figure 10: Ultrasonic microphone receiver circuit (top) and PCB (bottom) for capturing HUM signals. Our design may operate as a standalone receiver mounted aboard micro- and nano-drones.

5.2 Receiver Design: Acoustic Sensing

We use an acoustic sensor to decode the signal. We design and fabricate a miniature shield suitable for micro- and nano-drones. The shield includes a microphone and amplifier circuitry to capture the transmitted acoustic signals. We use a low-power bottom-port SPU0410LR5H analog MEMS microphone able to capture signals from 100 Hz to 80 kHz. The microphone package comprises an acoustic sensor, a low-noise input buffer, and an output amplifier [31]. It features a particularly high gain in the 10 kHz-30 kHz frequency region, where HUM transmits messages.

The complete schematics are shown at the top of Fig. 10. We use a 2-stage LMV358 operational amplifier featuring a rail-to-rail output swing [58]. We set the gain to 100 with a gain of 10 for each stage. We use a variable resistance potentiometer RV1 to set the signal level between the stages. We can set the bandwidth by choosing an appropriate value of C3 and C7, forming a pair of feedback capacitors. The LMV358 op-amp works well as a low-impedance driver/buffer. The output from the amplifier is fed to the ADC of the drone microcontroller for sampling. The fabricated PCB, shown at the bottom of Fig. 10, is 0.8 mm thick and measures 25×27 mm. It weighs a total of 1.8 g. The whole circuit consumes 0.75 mA while running at 3.3 V.

The microphone's bottom port is the acoustic inlet to receive the sound waves. The microphone is, therefore, susceptible to the noise propellers make. This necessitates the use of an insulating foam cover to mitigate this effect. We investigate the impact of different windscreens in Fig. 11, including a custom windscreen we fabricate using lightweight packaging foam to cover the microphone inlet. We create a specially designed 3D-printed cover that houses a curved 3 mm foam sheet to completely insulate the microphone from any peripheral wind from the propellers. The performance of the COTS windscreen is better at frequencies below 15 kHz. Our
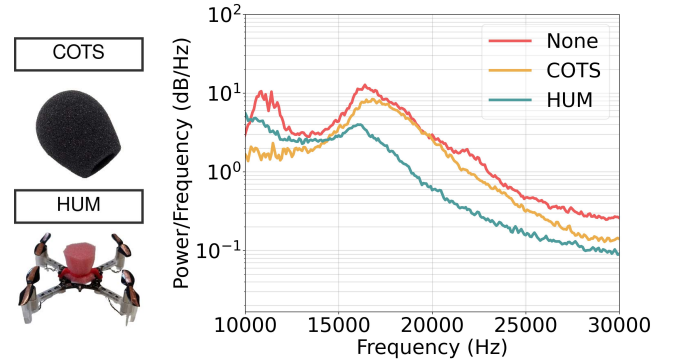

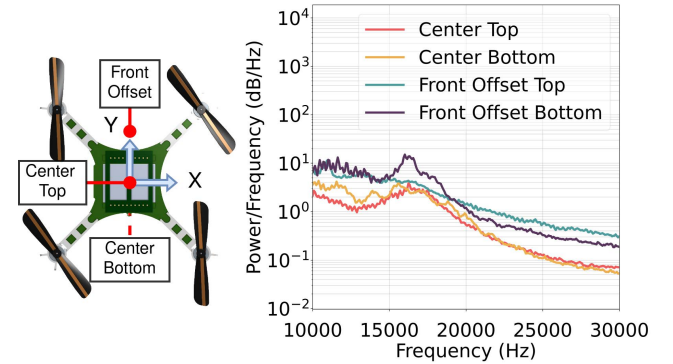Figure 11: Effect of different windscreens to mitigate propeller noise.

Figure 12: Effect of microphone position on the recorded noise power spectral density.

design outperforms the COTS configuration and all other options at higher frequencies.

Microphone placement with respect to the drone geometry is also crucial. We quantify the impact of this design choice as the drone flies in Fig. 12. The chart demonstrates that the most efficient placement is in the centre and on top of the drone, as it minimizes self-noise across the entire frequency band. The reason for this is that the propellers suck and push the air downwards; thus, there are regions near the propellers where airflow is turbulent, causing loud noise. We can limit the negative effects of this noise by placing the microphone on top and on par or higher than the propellers.

5.3 Orthogonal Channels and Decoding

We design a communication protocol using Binary Frequency Shift Keying (B-FSK) to encode the information over the acoustic channel. Several parameters are to be determined, as shown in Fig. 13.

We use two different *frequencies* for transmission f_{high} and f_{low}, each corresponding to two symbols. The higher frequency represents a '1' bit, and the lower frequency represents a '0' bit. The choice of frequency depends on operating distance, motors, and mechanical mounting. Based on Fig. 9, we choose a frequency corresponding to signals that quickly fade away, enabling communication only amongst co-located drones, or a frequency corresponding
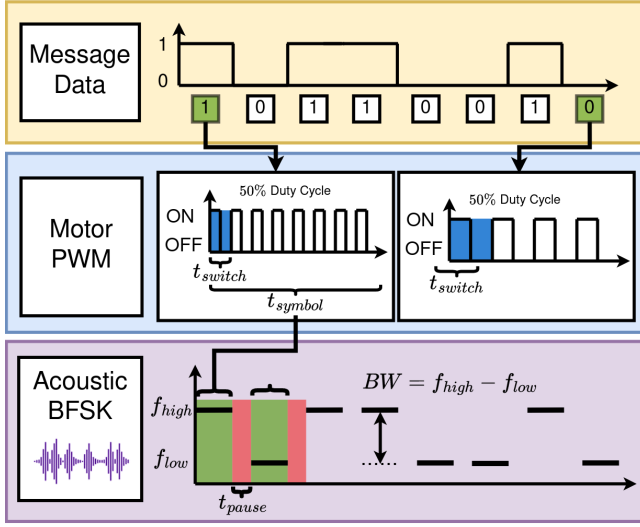
Figure 13: Binary Frequency Shift Keying communication scheme for encoding HUM messages.
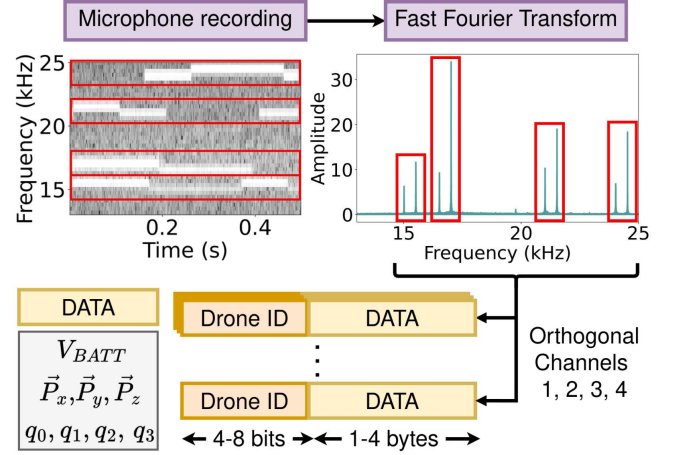

Figure 14: Simultaneous orthogonal audio frequency channels and on-board FFT decoding used by HUM to exchange coordination messages including position or quaternion vectors.

to signals that travel farther away, allowing communication in a larger area. The *bandwidth* is the difference between the two frequencies. We use a 1 kHz bandwidth. We choose this parameter to sufficiently separate simultaneous transmissions of different drones.

Symbol time is the period for transmitting a single symbol, which, in our case, corresponds to a single bit. The symbol time should be set to give the receiver enough time to detect a symbol successfully. The shorter the symbol time, the higher the data rate the system can achieve. We evaluate symbol times from 200 ms down to 25 ms. *Pause time* is the period between the transmission of two consecutive symbols, which is added to enable easier decoding of the BFSK signals by the receiver and has the opposite effect on data rates compared to symbol time. We can set a pause time of 0 ms between symbols and decode accurately.

On a quadrotor, *all four motors transmit different symbols*. Indeed, the acoustic waves we generate are between 15 kHz - 25 kHz, and the corresponding wavelength is larger than the inter-motor distance on the drone. This creates orthogonal channels at the receiver, enabling faster information exchange, as shown in Fig 14. An alternative may be to opt for four identical transmissions, improving SNR at the cost of reduced data rate. This option remains available to system designers, who can choose the above depending on application requirements and operating environment.

We decode the signals captured at 80 kHz which gives us a maximum working frequency of 40 kHz. We perform a Fast Fourier Transform (FFT) on a sliding window of samples. The window size is 512 samples, with the moving window progressing every 128 samples, taking 1.6 ms. We then perform FFT, which takes 0.52 ms on the STM32F4 micro-controller. This window size and sampling rate give us a bin resolution of 156.2 Hz, that is, a 6 value for each frequency and 12 in total for both f_{low} and f_{high} frequencies.

We then calculate the average signal around each symbol frequency. We compare these values and check if we observe a 2.2x

– 2.5x higher peak than the signal average. This threshold is determined empirically. If such a peak is found, we consider one bit symbol (0 or 1) to be detected. We count in successive windows how many such symbols we can find. If we detect the same symbol in at least 50% windows, each of them the duration of the symbol time, then we label that as a valid symbol. Otherwise, we discard it. If we encounter a stream of the same symbols, we split them and treat each separately since the system assumes that a symbol will not last longer than its configured symbol time.

Increasing the window size also causes the processing time of the signal to increase. The window size with 128 samples allows for a symbol time of 25 ms to be seen in at most 16 windows. We find that any symbol time duration lower than this makes distinguishing between noise and a valid symbol difficult. This gives us a maximum data rate of 40 bps for a single audio channel in HUM with a maximum of 160 bps per drone. This choice of communication parameters is dictated by the purview of maximizing the data rate and reducing the decoding errors while considering the limitations imposed by the decoding hardware.

6 EVALUATION

Our evaluation is two-pronged. We study the communication performance of HUM in Sec. 6.1, while we quantify the impact on drone dynamics, including battery life, in Sec. 6.2. Our evaluation is based on real flight tests on a nano UAV built using the CrazieFlie flight controller described earlier.

We use several different drones in our experiments, and each set of motors has slight variances in their internal resistance and physical construction. We verify that the motor tolerance variations do not impact the sound characteristics. The generated HUM is found to be consistent across these drones. Unless otherwise stated, we use 1 kHz bandwidth, 25 ms symbol time, and no pause time; we generate the signal per motor (channel) with a 50% transmitter
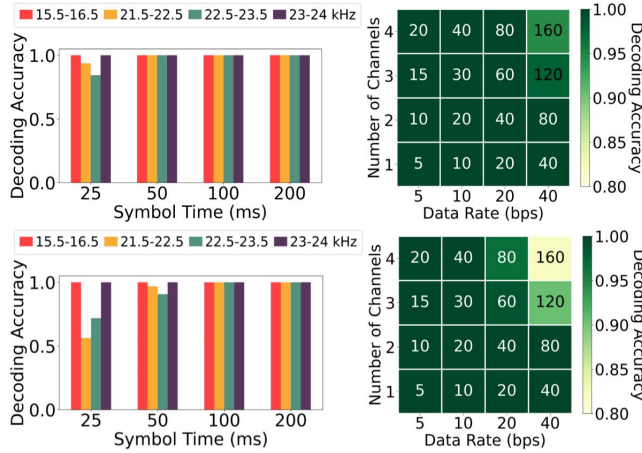
Figure 15: HUM decoding accuracy with varying BFSK symbol time along with the system data rate achieved when using multiple orthogonal prominent hum frequencies at close range (top) and far range (bottom).
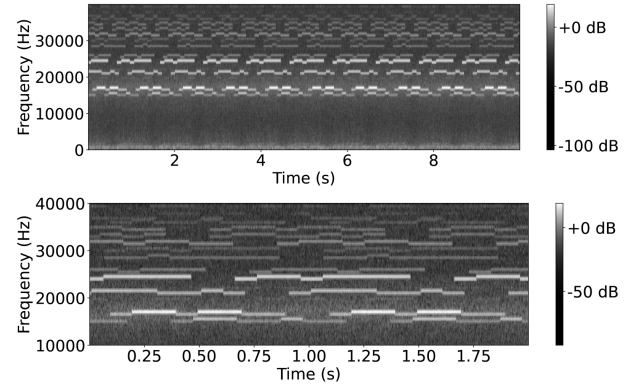

Figure 16: HUM acoustic spectrogram when 16 identical flying nano drones communicate simultaneously.

Figure 17: HUM decoding accuracy with varying distance between two flying drones when communicating.

duty cycle, and all are modified based on Sec. 4. We implement real-time communication in our tests and demonstrate its application towards drone coordination.

6.1 Communication Performance

We investigate HUM performance by measuring the captured signals' Bit Error Rate (BER) and decoding accuracy (1-BER). We vary key system parameters such as maximum data rate and number of simultaneous transmitters while evaluating the performance variation with different relative orientations and distances between transmitter and receiver. As for the latter, we consider two settings: a *close range* of 0.5 m and a *far range* of 3 m.

Varying symbol time and data rate. We can set different data rates by varying the symbol time. We keep 25 ms as the lower bound for this value, leading to a maximum data rate of 40 bps per channel, as explained in Sec.5.3. We see how the data varies with different transmission frequency pairs from 15 kHz up to 24 kHz which are chosen from the set of frequency bands with the highest intensity at higher distances, as discussed in Sec. 5.1.

Fig. 15 shows the decoding accuracy for each pair with varying separation between transmitter and receiver: close range (top) and far range (bottom). The prominent frequency pairs 15.5-16.5 kHz and 23-24 kHz perform better and can maintain a high decoding accuracy. We select these frequency pairs to further test the system. The system can achieve a maximum data rate of 160 bps with only 18% loss in accuracy using these frequencies. Lossless communication at 80 bps is possible in both ranges by selecting an appropriate set of frequency pairs.

Varying transmitters and distance. We evaluate how multiple nearby drones can simultaneously communicate. Each drone must be assigned a unique frequency pair to generate the HUM BFSK signals. Fig.16 shows the spectrogram when 16 drones flying in a 1.5 m radius simultaneously transmit their ID using HUM in the frequencies from 15 kHz to 35 kHz. We can successfully decode
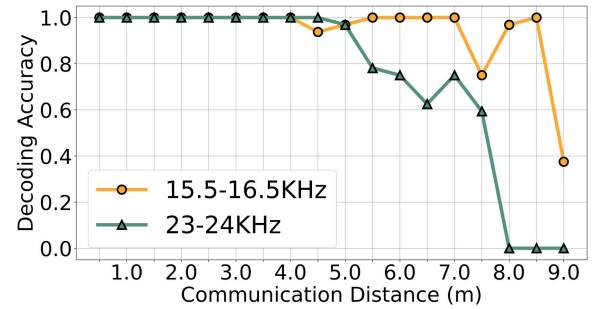
all 16 transmissions at a receiver drone flying in the centre of the circle using the process described earlier.

We measure the BER at varying distances to find the maximum communication range. We use a 40 bps data rate and increment the distance in steps of 0.5 m for the two most prominent frequency pairs. Fig. 17 shows that both frequency pairs can be decoded without errors up to a 4 m distance. We use HUM for drones flying up to an 8.5 m distance with the 15.5 kHz – 16.5 kHz frequency pair and a data rate up to 40 bps.

Varying orientation. We calculate the decoding accuracy with changing planar angles. Fig. 18 shows the results at a close range (left) and at a far range (right), using frequency pairs 15.5 kHz–16.5 kHz and 23 kHz–24 kHz. It shows that different transmitter-receiver angles slightly affect the decoding accuracy. The communication environment features metal cabinets, shelves, and boxes as shown in Fig. 20. This resulted in a loss of maximum decoding accuracy of 25%

We achieve the best angle performance in the far range when no surrounding occlusions exist. The lower-frequency pairs outperform the high-frequency ones for omnidirectional and environmentally neutral settings.

PWM duty cycle. As the drone flies, its PWM duty cycle is varied by the flight control logic depending on the desired maneuver. For CrazyFlie drones, we empirically learn that the drone hovers at a
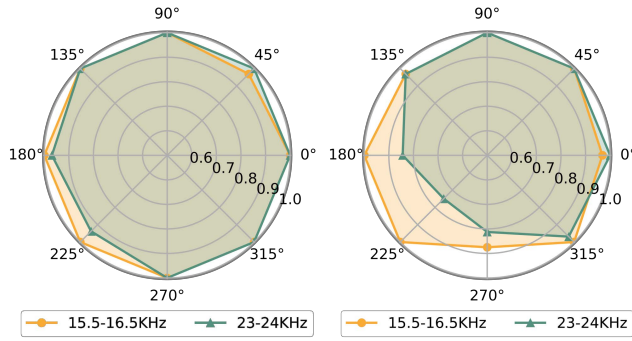
Figure 18: HUM decoding accuracy with varying angles between the transmitter and receiver drones at close range (left) and far range (right).
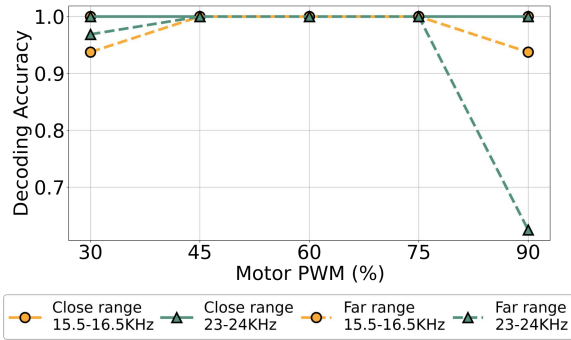

Figure 19: HUM decoding accuracy with varying PWM percentage of the HUM transmitting drone.

fixed altitude for PWM values between 45% and 75%. For values less than 45%, the drone descends, and for PWM greater than 75%, it ascends.

We evaluate the BER of the transmitting drone with varying PWM percentages. Fig. 19 depicts the close and far-range results. At close range, we observe a minimal effect of the transmitter PWM for both frequency pairs. The system works across PWM settings except those close to 0 or 100. This situation is transient, for example, when the drone is rapidly ascending or descending. Thus, around 45% to 75% PWM, the drones are hovering and performing their operation where HUM will help build the communication link better, which is useful.

Noise and space. We calculate the decoding accuracy in the presence of different ambient noise sources. Fig. 20 shows the results when the noise source is 0.5 m away from two drones communicating at close range using the frequency pairs 15.5 kHz–16.5 kHz and 23 KHz–24 kHz. The sources include common warehouse machine noises like drills, hammers, etc. Human speech and music were also included as potential sources of disturbance. As expected, different noise sources affect the two frequency pairs differently, although sufficient performance is achieved across all noise sources.

We test HUM with a group of 16 drones in a 4x4x3 m^3 flying cage, shown in Fig. 21. We consider two scenarios: one where the drones hover at the same altitude, that is, they are co-planar, and another
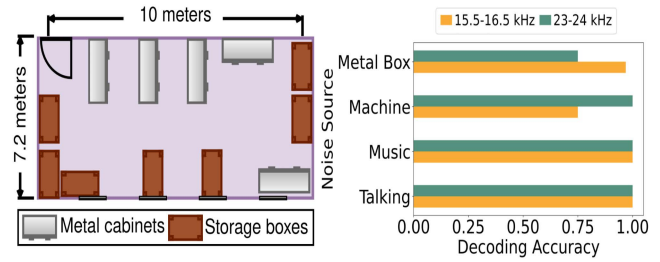
Figure 20: Floor map of the HUM communication test environment with metallic obstacles (left) and decoding accuracy with different ambient noise sources (right).
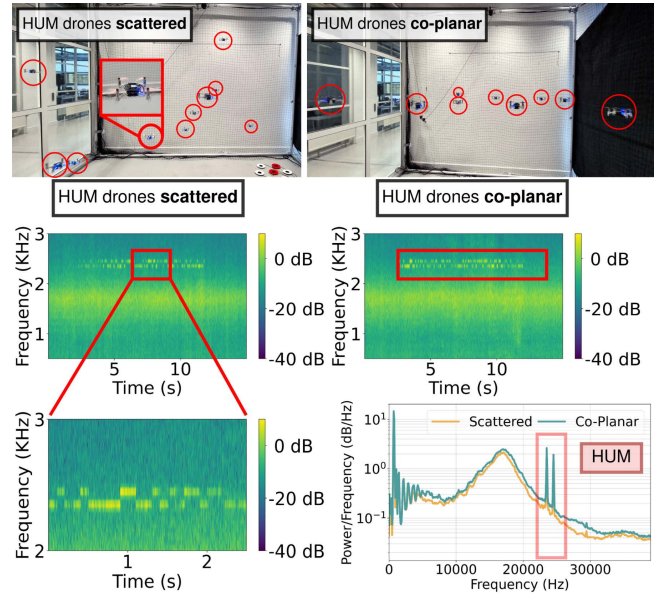
Figure 21: HUM operating with 16 identical flying CrazyFlies. The transmitting drone hovers in the middle while other drones hover at different altitudes scattered in 3D space or radially dispersed at the same altitude (co-planar). Spectrograms and power spectral density when HUM operates in either of the settings. This can be seen in [26].

one where they fly randomly scattered in three-dimensional space. Fig. 21 demonstrates that the noise intensity is much higher when the drones are co-planar than in the other scenario. However, in both cases, HUM captures and decodes messages successfully.

6.2 Drone Dynamics

We consider the effect of HUM on the drone dynamics. This involves measuring pitch, roll, yaw stability, generated thrust, and impact on battery life. We show the impact of the HUM system on the drone's attitude and dynamics.

Thrust. We evaluate the effect of HUM on the thrust generated for a varying PWM duty cycle. We use a weight scale with a custom 3D-printed mount to measure the thrust produced by the drone using all four motors, both when the drone motors constantly produce

Figure 22: Generated thrust with varying PWM (top) and with different number of motors transmitting HUM communication (bottom).

Figure 23: Variation of the pitch, roll, and yaw angles when the drone uses COTS and modified propellers. The green region shows when the HUM communication system is turned on.

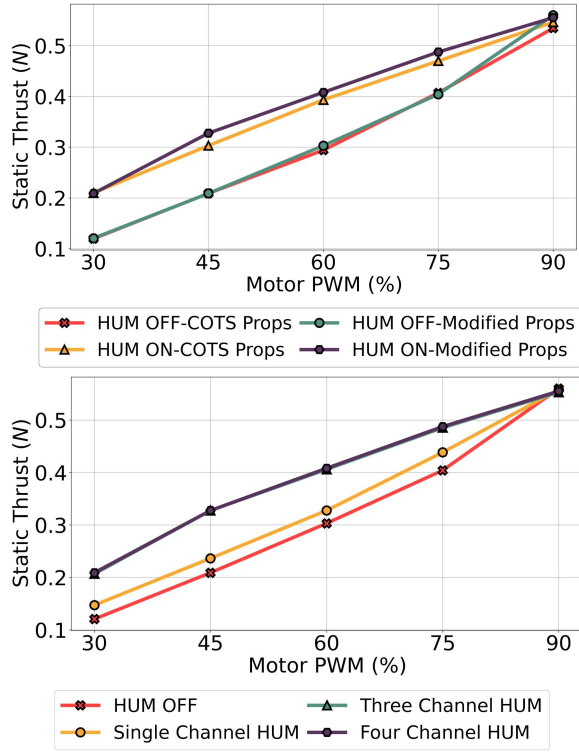Figure 24: Drone battery life with varying PWM percentages when using HUM communication with COTS and modified propellers.

the HUM signals and when they are powered on. We test the two scenarios with both COTS propellers and our modified propellers.

The top graph in Fig. 22 shows that the modified propellers have a net positive effect on the generated thrust. This increase only amounts to 0.024 N in the worst case for 45% PWM duty cycle. Using HUM, however, does seem to increase the net thrust produced using propellers. This could be a consequence of temporarily increasing the power input to the motors because of humming.

The bottom chart in Fig. 22 reports how the thrust varies when humming with a different number of motors. As expected, the thrust increases when more motors are humming simultaneously, yet no significant difference in thrust is produced when three or all four motors communicate using HUM. However, the increase that does occur is only 0.1 N in the worst case. This is insignificant since, in practice, we do not constantly transmit HUM signals but only in short bursts whenever necessary. Nevertheless, we further evaluate the effect of these spikes by testing the drone attitude stability with HUM communication.

Attitude stability. We use the stock flight control system of the CrazyFlie and the open source 3 degrees of freedom, Open Gimbal [51]. This allows us to analyze the effect of the motor transmissions and the propeller modification that HUM requires to operate. We record the roll, pitch, and yaw angles at a sampling rate of 100 Hz. Every experiment starts with the batteries fully charged. We set it at 75% PWM duty cycle and generate a constant hum at

22 kHz. We let the drone stabilize for the first 5 s in an experiment without humming to establish the baseline, and then we transmit hum signals for another 5 s. Fig. 23 shows the results. HUM only affects the roll and pitch axes by a maximum of 2.5° when using the modified propellers and affects the yaw axis by only 0.1°, which can be easily compensated by tuning the PID control parameters to account for these angular deviations.

Battery life. We measure the battery life when using our modified propellers on the HUM system for communication. We compare this figure with the CrazyFlie firmware release tag 2023.07 as the baseline. The drones send HUM signals at 5 Hz after startup and we use the same battery to maintain uniformity in results. Fig. 24 shows the results. The graph shows two factors our system introduced that can potentially drain battery life: propeller modification and motor HUM signalling. We indicate these using the terns HUM ON/OFF and COTS/modified propellers. Our modified propellers result in a small net decrease in battery life compared to the baseline, regardless of whether the drone uses HUM. The decrease also differs with PWM, with a maximum of 4% change at the 60% PWM duty cycle. Crucially, when using HUM, the worst-case battery penalty is limited to 7%. Again, this is when the drone transmits updates continuously using the side channel, which is not typical. As such, in practice HUM would only be used to coordinate and send important information occasionally.

7 DISCUSSION

We provide additional insights regarding the design choices, the applicability of HUM, and how it compares with existing techniques.

Applications. We maintain that HUM enables applications that would otherwise be unfeasible using side-channel non-RF communications. We hinted in the Introduction at several motivating examples. Let us offer a precise quantitative perspective here, linked with the drone identification system we mentioned.

The drone identifier currently mandated by European drone regulations is at least 12 bytes [20]. Using Bleep [10], a drone that communicates its identification to nearby flying devices, for example, to avoid collisions in shared airspace, takes 48 s to do so. This time is way excessive to avoid collisions [44, 63]. Transmitting the same amount of data with HUM is *achieved in 0.6 s*, which is sufficient to react according to the identifier of the other party. With higher processing power, the bit rate can also be increased further.

The 80x higher data rates than Bleep [10] fundamentally change the target application domains. HUM allows drones to use non-RF side-channel communications to transmit rich information, such as information for coordination among multiple drones [44, 63], for example, to maintain flight formation. Unlike Bleep, the few bits per second provided by Bleep mainly allow periodic "heartbeats" to be transmitted, which do not convey much more information than the transmitting drone still exists.

Longterm impact and stability. We modify the propeller's physical design. A potential concern is that this can have unexpected long-term consequences on drone stability and the motor lifetime. The modifications to eliminate self-interference are based on the idea that simple design changes to propellers can improve communication performance. Further, the modifications are nondestructive and easily reversible, making their usage simple and applicable on an ad-hoc basis to existing drones.

The idea is to eventually have these modifications a natural part of the drones carrying HUM receivers. Based on our early assessment, the motors' lifetime is not impacted by HUM signaling but requires further prolonged studies to validate. As we find that our changes do not severely affect two key drone flight parameters, that is, generated thrust and attitude dynamics, impacts on the long-term stability of the drone are unlikely to occur.

Performance. Our tests are dynamic, conducted with drones at various distances navigating confined spaces and predetermined paths to ensure collision avoidance. Movements induce *Doppler* effects, with a worst-case shift of approximately 50 Hz at a relative velocity of 1 m/s, constituting less than 5% of the bandwidth. Doppler variation can be managed by hovering, adjusting data rates, or widening the frequency gap between f_{lower} and f_{higher}.

Our focus is on *localized* drone-to-drone communication. Our experiments indicate a maximum operational range of 8.5 m, shown in Fig. 17, which is adequate for localized data exchanges, including position, attitude, and sensor data, crucial for most *decentralized* drone coordination systems [44, 63]. Multi-hop communication may be layered on top of primitive HUM communication to extend the range, adapting existing protocols. Once again, this is only possible because the provided data rates may allow the exchange of control messages with reasonable latency, which is instead unfeasible with rates of a few bits per second [10].

Drone size. We may, in principle, implement HUM on larger drones with the only requirement that the motors be powered with a set PWM frequency rather than DC power. Larger drones increase the communication range. The larger a drone is, the louder its motors are. This is a consequence of more current flowing through the motors and the dimensions of the motor casing itself. While the relationship between drone size and the produced HUM intensity is not linear, it will certainly show a positive trend. Thus, the communication distance can scale with drone size. However, the larger drones also need to have higher spacing between them. But the energy requirements for HUM receivers will remain the same irrespective of size. We focused on micro- and nano-drones, as they represent enabling factors in the target applications and represent a challenging case to study due to resource constraints.

The CrazyFlie only hovers stably for a PWM duty cycle of around 45-75%. Above these values, the drone starts to gain or lose altitude. We can still use HUM if the PWM is not greater than 95%. Settings close to 100% PWM duty cycle are only rarely encountered, and even then, only for a short period, for example, when the drone must rapidly gain altitude. Modifying drone speeds during transmission presents challenges due to adjusted PWM parameters, as in Fig. 19.

8 CONCLUSION

Drone teams require localized communications through a non-RF side channel. We design HUM precisely to this end. Based on a deep understanding of how and where noise is generated on a drone, we designed a propeller modification to reduce noise by taking inspiration from the wing features of barn owls. Using a custom ultrasonic microphone shield, we use the drone motor's PWM switching frequency to transmit simultaneous orthogonal channels decoded on board. HUM's improved signal-to-noise ratio enables 80x higher data rates than existing designs while providing better overall scalability. We evaluated the design of HUM, its dynamic behavior, and its communication performance in a real setting. HUM can support simultaneous decoding across 16 drones within an 8 m range, yet the impact on battery life is a mere 7% overhead in the worst case. Further, we want to study how to increase the bit rate using different signal processing techniques while trading off with respect to processing power and energy consumption.

REFERENCES

[1] 2015. Crazyflie Firmware Repository. https://github.com/bitcraze/crazyflie-firmware/commits/master/src/modules/src/sound_cf2.c

[2] 2023. EspressIF ESPDrone. https://docs.espressif.com/projects/espressif-esp-drone/en/latest/gettingstarted.html

[3] 2024. Remote Identification of Drones | Federal Aviation Administration. https://www.faa.gov/uas/getting_started/remote_id

[4] Mikhail Afanasov, Alessandro Djordjevic, Feng Lui, and Luca Mottola. 2019. Fly-Zone: A testbed for experimenting with aerial drone applications. In *Proceedings of the 17th Annual International Conference on Mobile Systems, Applications, and Services*. 67–78.

[5] Saeed H Alsamhi, Ou Ma, Mohammad Samar Ansari, and Faris A Almalki. 2019. Survey on collaborative smart drones and internet of things for improving smartness of smart cities. *Ieee Access* 7 (2019), 128125–128152.

[6] Riham Altawy and Amr M Youssef. 2016. Security, privacy, and safety aspects of civilian drones: A survey. *ACM Transactions on Cyber-Physical Systems* 1, 2 (2016), 1–25.

[7] Hadi Ardiny and Amir Mohammad Beigzadeh. 2024. Enhancing radioactive environment exploration with bio-inspired swarm robotics: A comparative analysis of Lévy flight and stigmergy methods. *Robotics and Autonomous Systems* 181 (11 2024), 104794. https://doi.org/10.1016/J.ROBOT.2024.104794

[8] Dmitri Asonov and Rakesh Agrawal. 2004. Keyboard acoustic emanations. In *IEEE Symposium on Security and Privacy, 2004. Proceedings. 2004*. IEEE, 3–11.

[9] Michael Backes, Markus Dürmuth, Sebastian Gerling, Manfred Pinkal, Caroline Sporleder, et al. 2010. Acoustic {Side-Channel} attacks on printers. In *19th USENIX Security Symposium (USENIX Security 10)*.

[10] Adeola Bannis, Hae Young Noh, and Pei Zhang. 2020. Bleep: motor-enabled audio side-channel for constrained UAVs. In *Proceedings of the 26th Annual International Conference on Mobile Computing and Networking (MobiCom '20)*. Association for Computing Machinery, 1–13.

[11] Jody Berger and Josie Garthwaite. 2021. Lessons from Fukushima disaster 10 years later | Stanford Report. https://news.stanford.edu/stories/2021/03/lessons-fukushima-disaster-10-years-later

[12] Bitcraze AB 2021. *Crazyflie 2.1*. Bitcraze AB. Rev. 3.

[13] Rafael G. Braga, Roberto C. da Silva, Alexandre C. B. Ramos, and Felix Mora-Camino. 2017. UAV swarm control strategies: A case study for leak detection. In *2017 18th International Conference on Advanced Robotics (ICAR)*. 173–178. https://doi.org/10.1109/ICAR.2017.8023514

[14] E. Bregu et al. 2016. Reactive Control of Autonomous Drones. In *Proceedings of ACM MobiSys, Singapore, June 26-30, 2016*.

[15] Zhihao Chen, Chao Liu, Ekta Rani, Harishchandra Singh, Marko Huttula, Jukka Kömi, and Wei Cao. 2021. Ultrasonic vibration-induced severe plastic deformation of Cu foils: effects of elastic-plastic stress wave bounce, acoustic softening, and size effect. *The International Journal of Advanced Manufacturing Technology* 115, 11 (2021), 3617–3629.

[16] Asaf Cidon, Kanthi Nagaraj, Sachin Katti, and Pramod Viswanath. 2012. Flashback: decoupled lightweight wireless control. In *Proceedings of the ACM SIGCOMM 2012 Conference on Applications, Technologies, Architectures, and Protocols for Computer Communication (Helsinki, Finland) (SIGCOMM '12)*. Association for Computing Machinery, New York, NY, USA, 223–234. https://doi.org/10.1145/2342356.2342400

[17] Radu Curpen, Titus Bălan, Ioan Alexandru Micloș, and Ionut Comănici. 2018. Assessment of signal jamming efficiency against LTE UAVs. In *2018 International Conference on Communications (COMM)*. IEEE, 367–370.

[18] DSV. 2020. DSV improves warehouse operations with drone system. https://www.youtube.com/watch?v=5N87L_nO2ms&t=49s

[19] Sara Eriksson, Åsa Unander-Scharin, Vincent Trichon, Carl Unander-Scharin, Hedvig Kjellström, and Kristina Höök. 2019. Dancing with drones: Crafting novel artistic expressions through intercorporeality. In *Proceedings of the 2019 CHI Conference on Human Factors in Computing Systems*. 1–12.

[20] European Union Aviation Safety Agency. 2024. Easy Access Rules for Unmanned Aircraft Systems (Regulation (EU) 2019/947 and Regulation (EU) 2019/945). https://www.easa.europa.eu/en/downloads/110913/en

[21] Dario Floreano and Robert J Wood. 2015. Science, technology and the future of small autonomous drones. *Nature* 521, 7553 (2015), 460.

[22] Ming Gao, Feng Lin, Weiye Xu, Muertikepu Nuermaimaiti, Jinsong Han, Wenyao Xu, and Kui Ren. 2020. Deaf-aid: mobile IoT communication exploiting stealthy speaker-to-gyroscope channel. In *Proceedings of the 26th Annual International Conference on Mobile Computing and Networking*. 1–13.

[23] Lav Gupta, Raj Jain, and Gabor Vaszkun. 2016. Survey of Important Issues in UAV Communication Networks. *IEEE Communications Surveys & Tutorials* 18, 2 (2016), 1123–1152. https://doi.org/10.1109/COMST.2015.2495297

[24] Timothy Hornyak. 2016. How robots are becoming critical players in nuclear disaster cleanup | Science | AAAS. https://www.science.org/content/article/how-robots-are-becoming-critical-players-nuclear-disaster-cleanup

[25] Harvey H Hubbard. 1991. *Aeroacoustics of flight vehicles: theory and practice*. Vol. 1. National Aeronautics and Space Administration, Office of Management.

[26] HUM. 2024. *HUM video demonstration*. https://youtu.be/Ji_CjWFnaB4

[27] Vikram Iyer, Maruchi Kim, Shirley Xue, Anran Wang, and Shyamnath Gollakota. 2020. *Airdropping Sensor Networks from Drones and Insects*. Association for Computing Machinery, New York, NY, USA.

[28] Justin W Jaworski and Nigel Peake. 2020. Aeroacoustics of silent owl flight. *Annual Review of Fluid Mechanics* 52 (2020), 395–420.

[29] Song Min Kim and Tian He. 2015. FreeBee: Cross-technology Communication via Free Side-channel. In *Proceedings of the 21st Annual International Conference on Mobile Computing and Networking (Paris, France) (MobiCom '15)*. Association for Computing Machinery, New York, NY, USA, 317–330. https://doi.org/10.1145/2789168.2790098

[30] Younghyun Kim, Woo Suk Lee, Vijay Raghunathan, Niraj K. Jha, and Anand Raghunathan. 2015. Vibration-Based Secure Side Channel for Medical Devices. In *Proceedings of the 52nd Annual Design Automation Conference (San Francisco, California) (DAC '15)*. Association for Computing Machinery, New York, NY, USA, Article 32, 6 pages. https://doi.org/10.1145/2744769.2744928

[31] Knowles 2013. *Zero-Height SiSonic Microphone*. Knowles. Rev. H.

[32] Angus Leslie, Kee Choon Wong, and Doug Auld. 2008. Broadband noise reduction on a mini-UAV propeller. In *14th AIAA/CEAS Aeroacoustics Conference (29th AIAA Aeroacoustics Conference)*. 3069.

[33] Jian Liu, Yan Wang, Gorkem Kar, Yingying Chen, Jie Yang, and Marco Gruteser. 2015. Snooping keystrokes with mm-level audio ranging on a single phone. In *Proceedings of the 21st Annual International Conference on Mobile Computing and Networking*. 142–154.

[34] Reda R Mankbadi, Samuel Afari, and Vladimir V Golubev. 2020. Simulations of broadband noise of a small uav propeller. In *AIAA Scitech 2020 Forum*. 1493.

[35] Dubravko Miljković. 2018. Methods for attenuation of unmanned aerial vehicle noise. In *2018 41st International Convention on Information and Communication Technology, Electronics and Microelectronics (MIPRO)*. 0914–0919. https://doi.org/10.23919/MIPRO.2018.8400169

[36] Abdirahman Mohamud and Ashwin Ashok. 2018. Drone noise reduction through audio waveguiding. In *Proceedings of the 4th ACM Workshop on Micro Aerial Vehicle Networks, Systems, and Applications*. 92–94.

[37] Luca Mottola, Mattia Moretta, Kamin Whitehouse, and Carlo Ghezzi. 2014. Team-level programming of drone sensor networks. In *Proceedings of the 12th ACM Conference on Embedded Network Sensor Systems*. 177–190.

[38] Luca Mottola and Kamin Whitehouse. 2017. Mobile systems research with drones. *GetMobile: Mobile Computing and Communications* 20, 4 (2017), 17–22.

[39] Rajalakshmi Nandakumar, Krishna Kant Chintalapudi, Venkat Padmanabhan, and Ramarathnam Venkatesan. 2013. Dhwani: secure peer-to-peer acoustic NFC. *ACM SIGCOMM Computer Communication Review* 43, 4 (2013), 63–74.

[40] Mustafa Melikşah Özmen and Bekir Aksoy. 2023. An example application for an identification of friend and foe (IFF) system appropriate for unmanned aerial vehicles (UAV) based on deep learning. *Journal of Intelligent & Robotic Systems* 107, 3 (2023), 36.

[41] Federico Petricelli, Paruchuri Chaitanya, Sergi Palleja-Cabre, Stefano Meloni, Phillip F Joseph, Amin Karimian, Suresh Palani, and Roberto Camussi. 2023. An experimental investigation on the effect of in-flow distortions of propeller noise. *Applied Acoustics* 214 (2023), 109682.

[42] Sixu Piao, Zhongjie Ba, Lu Su, Dimitrios Koutsonikolas, Shi Li, and Kui Ren. 2019. Automating csi measurement with uavs: from problem formulation to energy-optimal solution. In *IEEE INFOCOM 2019-IEEE Conference on Computer Communications*. IEEE, 2404–2412.

[43] James A. Preiss, Wolfgang Honig, Gaurav S. Sukhatme, and Nora Ayanian. 2017. Crazyswarm: A large nano-quadcopter swarm. In *2017 IEEE International Conference on Robotics and Automation (ICRA)*. 3299–3304. https://doi.org/10.1109/ICRA.2017.7989376

[44] James A. Preiss, Wolfgang Honig, Gaurav S. Sukhatme, and Nora Ayanian. 2017. Crazyswarm: A large nano-quadcopter swarm. In *2017 IEEE International Conference on Robotics and Automation (ICRA)*. 3299–3304. https://doi.org/10.1109/ICRA.2017.7989376

[45] Aveek Purohit, Zheng Sun, Frank Mokaya, and Pei Zhang. 2011. SensorFly: Controlled-mobile sensing platform for indoor emergency response applications. In *Proceedings of the 10th ACM/IEEE International Conference on Information Processing in Sensor Networks*. IEEE, 223–234.

[46] Yujie Qian, Yuliang Wei, Deyi Kong, and He Xu. 2021. Experimental investigation on motor noise reduction of Unmanned Aerial Vehicles. *Applied Acoustics* 176 (2021), 107873.

[47] Jacek Rak, David Hutchison, Janos Tapolcai, Rasa Bruzgiene, Massimo Tornatore, Carmen Mas-Machuca, Marija Furdek, and Paul Smith. 2020. Fundamentals of communication networks resilience to disasters and massive disruptions. *Guide to disaster-resilient communication networks* (2020), 1–43.

[48] Soundarya Ramesh, Thomas Pathier, and Jun Han. 2019. SoundUAV: Finger-printing Acoustic Emanations for Delivery Drone Authentication (Poster). In *Proceedings of the 17th Annual International Conference on Mobile Systems, Applications, and Services (Seoul, Republic of Korea) (MobiSys '19)*. Association for Computing Machinery, New York, NY, USA, 632–633. https://doi.org/10.1145/3307334.3328662

[49] Ralph Restituyo and Thaier Hayajneh. 2018. Vulnerabilities and attacks analysis for military and commercial iot drones. In *2018 9th IEEE Annual Ubiquitous Computing, Electronics & Mobile Communication Conference (UEMCON)*. IEEE, 26–32.

[50] Himmat Singh Sandhu and Siddhartha Raja. 2019. *No Broken Link: The Vulnerability of Telecommunication Infrastructure to Natural Hazards.* World Bank.

[51] Suryansh Sharma, Tristan Dijkstra, and R Venkatesha Prasad. 2023. Open Gimbal: A 3 Degrees of Freedom Open Source Sensing and Testing Platform for Nano and Micro UAVs. *IEEE Sensors Letters* (2023).

[52] Suryansh Sharma, Ashutosh Simha, Venkatesha Prasad, Shubham Deshmukh, Kavin Balaji Saravanan, Ravi Ramesh, and Luca Mottola. 2023. BEAVIS: Balloon Enabled Aerial Vehicle for IoT and Sensing. In *Proceedings of the 29th Annual International Conference on Mobile Computing and Networking.* 1–15.

[53] Xiufang Shi, Chaoqun Yang, Weige Xie, Chao Liang, Zhiguo Shi, and Jiming Chen. 2018. Anti-drone system with multiple surveillance technologies: Architecture, implementation, and challenges. *IEEE Communications Magazine* 56, 4 (2018), 68–74.

[54] Alex Stoll. 2012. *Design of quiet UAV propellers.* Stanford University.

[55] Yimiao Sun, Weiguo Wang, Luca Mottola, Ruijin Wang, and Yuan He. 2023. AIM: Acoustic Inertial Measurement for Indoor Drone Localization and Tracking. In *Proceedings of the 20th ACM Conference on Embedded Networked Sensor Systems* (Boston, Massachusetts) *(SenSys '22).* Association for Computing Machinery, New York, NY, USA, 476–488. https://doi.org/10.1145/3560905.3568499

[56] Hartmut Surmann, Tiffany Kaiser, Artur Leinweber, Gerhard Senkowski, Dominik Slomma, and Marc Thurow. 2021. Small Commercial UAVs for Indoor Search and Rescue Missions. In *IEEE International Conference on Automation, Robotics and Applications.* 106–113.

[57] Lina Tang and Guofan Shao. 2015. Drone remote sensing for forestry research and practices. *Journal of Forestry Research* 26 (2015), 791–797.

[58] Texas Instruments 2023. *LMV3xx Low-Voltage Rail-to-Rail Output Operational Amplifier.* Texas Instruments. Rev. Y.

[59] Teodor Tomic, Korbinian Schmid, Philipp Lutz, Andreas Domel, Michael Kassecker, Elmar Mair, Iris Lynne Grixa, Felix Ruess, Michael Suppa, and Darius Burschka. 2012. Toward a fully autonomous UAV: Research platform for indoor and outdoor urban search and rescue. *IEEE robotics & automation magazine* 19, 3 (2012), 46–56.

[60] Kenneth W. Van Treuren and Charles F. Wisniewski. 2019. Testing Propeller Tip Modifications to Reduce Acoustic Noise Generation on a Quadcopter Propeller. *Journal of Engineering for Gas Turbines and Power* 141, 12 (11 2019), 121017. https://doi.org/10.1115/1.4044971 arXiv:https://asmedigitalcollection.asme.org/gasturbinespower/article-pdf/141/12/121017/6448668/gtp_141_12_121017.pdf

[61] Kenneth W Van Treuren and Charles F Wisniewski. 2019. Testing propeller tip modifications to reduce acoustic noise generation on a quadcopter propeller. *Journal of Engineering for Gas Turbines and Power* 141, 12 (2019), 121017.

[62] Gurkan Tuna, Bilel Nefzi, and Gianpaolo Conte. 2014. Unmanned aerial vehicle-aided communications system for disaster recovery. *Journal of network and computer Applications* 41 (2014), 27–36.

[63] Gábor Vásárhelyi, Csaba Virágh, Gergő Somorjai, Tamás Nepusz, Agoston E Eiben, and Tamás Vicsek. 2018. Optimized flocking of autonomous drones in confined environments. *Science Robotics* 3, 20 (2018), eaat3536.

[64] Weiguo Wang, Jinming Li, Yuan He, Xiuzhen Guo, and Yunhao Liu. 2022. Motor-Beat: Acoustic Communication for Home Appliances via Variable Pulse Width Modulation. *Proceedings of the ACM on Interactive, Mobile, Wearable and Ubiquitous Technologies* 6, 1 (2022), 1–24.

[65] Weiguo Wang, Luca Mottola, Yuan He, Jinming Li, Yimiao Sun, Shuai Li, Hua Jing, and Yulei Wang. 2023. MicNest: Long-Range Instant Acoustic Localization of Drones in Precise Landing. In *Proceedings of the 20th ACM Conference on Embedded Networked Sensor Systems* (Boston, Massachusetts) *(SenSys '22).* Association for Computing Machinery, New York, NY, USA, 504–517. https://doi.org/10.1145/3560905.3568515

[66] Ware. 2020. Automating cycle counting with warehouse drones at CEVA Logistics | Ware. https://www.youtube.com/watch?v=nV34cMDfu_0

[67] Yuliang Wei, Feng Xu, Shiyuan Bian, and Deyi Kong. 2020. Noise reduction of UAV using biomimetic propellers with varied morphologies leading-edge serration. *Journal of Bionic Engineering* 17 (2020), 767–779.

[68] Kaishun Wu, Haoyu Tan, Yunhuai Liu, Jin Zhang, Qian Zhang, and Lionel Ni. 2010. Side channel: bits over interference. In *Proceedings of the Sixteenth Annual International Conference on Mobile Computing and Networking* (Chicago, Illinois, USA) *(MobiCom '10).* Association for Computing Machinery, New York, NY, USA, 13–24. https://doi.org/10.1145/1859995.1859998

[69] American Physical Society X. 2013. The secrets of owls' near Noiseless Wings. https://phys.org/news/2013-11-secrets-owls-noiseless-wings.html

[70] Xiangyu Xu, Jiadi Yu, Yingying Chen, Yanmin Zhu, Linghe Kong, and Minglu Li. 2019. BreathListener: Fine-Grained Breathing Monitoring in Driving Environments Utilizing Acoustic Signals. In *Proceedings of the 17th Annual International Conference on Mobile Systems, Applications, and Services* (Seoul, Republic of Korea) *(MobiSys '19).* Association for Computing Machinery, New York, NY, USA, 54–66. https://doi.org/10.1145/3307334.3326074

[71] Sangki Yun, Yi-Chao Chen, Huihuang Zheng, Lili Qiu, and Wenguang Mao. 2017. Strata: Fine-Grained Acoustic-Based Device-Free Tracking. In *Proceedings of the 15th Annual International Conference on Mobile Systems, Applications, and Services* (Niagara Falls, New York, USA) *(MobiSys '17).* Association for Computing Machinery, New York, NY, USA, 15–28. https://doi.org/10.1145/3081333.3081356

[72] Maotian Zhang, Ping Li, Panlong Yang, Jie Xiong, and Chang Tian. 2016. Poster: Sonicnect: Accurate Hands-Free Gesture Input System with Smart Acoustic Sensing. In *Proceedings of the 14th Annual International Conference on Mobile Systems, Applications, and Services Companion* (Singapore, Singapore) *(MobiSys '16 Companion).* Association for Computing Machinery, New York, NY, USA, 91. https://doi.org/10.1145/2938559.2948830

[73] Bing Zhou, Mohammed Elbadry, Ruipeng Gao, and Fan Ye. 2017. BatMapper: Acoustic Sensing Based Indoor Floor Plan Construction Using Smartphones. In *Proceedings of the 15th Annual International Conference on Mobile Systems, Applications, and Services* (Niagara Falls, New York, USA) *(MobiSys '17).* Association for Computing Machinery, New York, NY, USA, 42–55. https://doi.org/10.1145/3081333.3081363

[74] Manfu Zhu and Liran Ma. 2024. A review of recent advances in the effects of surface and interface properties on marine propellers. *Friction* 12, 2 (2024), 185–214.

[75] Yulong Zou, Jia Zhu, Tonghua Wu, Haiyan Guo, and Hao Wei. 2021. Cooperative Drone Communications for Space-Air-Ground Integrated Networks. *IEEE Network* 35, 5 (2021), 100–106. https://doi.org/10.1109/MNET.111.2100016